HOKKAIDO UNIVERSITY

Title	High drug efflux pump capacity and low DNA damage response induce doxorubicin resistance in canine hemangiosarcoma cell lines
Author(s)	Morita, Atsuya; Aoshima, Keisuke; Gulay, Kevin Christian Montecillo; Onishi, Shinichi; Shibata, Yuki; Yasui, Hironobu; Kobayashi, Atsushi; Kimura, Takashi
Citation	Research in veterinary science, 127, 1-10 https://doi.org/10.1016/j.rvsc.2019.09.011
Issue Date	2019-12
Doc URL	http://hdl.handle.net/2115/79880
Rights	© 2019. This manuscript version is made available under the CC-BY-NC-ND 4.0 license https://creativecommons.org/licenses/by-nc-nd/4.0/
Rights(URL)	https://creativecommons.org/licenses/by-nc-nd/4.0/
Type	article (author version)
File Information	manuscript.pdf

Instructions for use

Hokkaido University Collection of Scholarly and Academic Papers : HUSCAP

Original Research

Title

High drug efflux pump capacity and low DNA damage response induce doxorubicin resistance in canine hemangiosarcoma cell lines

Author names

Atsuya Morita[1], Keisuke Aoshima[1*], Kevin Christian Montecillo Gulay[1], Shinichi Onishi[1], Yuki Shibata[2], Hironobu Yasui[3], Atsushi Kobayashi[1], Takashi Kimura[1]

Authors' affiliations

[1]Laboratory of Comparative Pathology, Department of Clinical Veterinary Sciences, Faculty of Veterinary Medicine, Hokkaido University, Sapporo, Hokkaido 060-0818 Japan

[2]Laboratory of Integrated Molecular Imaging, Department of Biomedical Imaging, Graduate School of Biomedical Science and Engineering, Hokkaido University, Sapporo, Hokkaido 060-8638 Japan

[3]Laboratory of Radiation Biology, Department of Applied Veterinary Sciences, Faculty of Veterinary Medicine, Hokkaido University, Sapporo, Hokkaido 060-0818, Japan

*To whom correspondence should be addressed: Keisuke Aoshima, Laboratory of Comparative Pathology, Department of Clinical Veterinary Sciences, Faculty of Veterinary medicine, Hokkaido University, Kita 18 Nishi 9, Kita-ku, Sapporo, Hokkaido 060-0818 Japan; k-aoshima@vetmed.hokudai.ac.jp; Tel. +81-11- 706-5193, FAX. +81-11-706-5194

Abstract

Canine hemangiosarcoma (HSA) is an aggressive malignant endothelial tumor in dogs and characterized by poor prognosis because of its high invasiveness, high metastatic potential, and poor responsiveness to anti-cancer drugs. Although doxorubicin-based chemotherapy is regularly conducted after surgical treatment, its effects on survival rates are limited. Acquisition of drug resistance is one of the causes of this problem, but the underlying mechanisms remain unclear. In the present study, we aimed to identify the drug-resistance mechanism in canine HSA by establishing doxorubicin-resistant (DR) HSA cell lines. HSA cell lines were exposed to doxorubicin at gradually increasing concentrations. When the cells were able to grow in the presence of a 16-fold higher doxorubicin concentration compared with the initial culture, they were designated DR-HSA cell lines. Characterization of these DR-HSA cell lines revealed higher drug efflux pump capacity compared with the parental cell lines. Furthermore,

the DR-HSA cell lines did not show activation of the DNA damage response despite carrying high DNA damage burdens, meaning that apoptosis was not strongly induced. In conclusion, canine HSA cell lines acquired doxorubicin resistance by increasing their drug efflux pump capacity and decreasing the DNA damage response. This study provides useful findings to promote further research on the drug-resistance mechanisms in canine HSA.

Keywords

Apoptosis, Cancer, DNA damage response, Doxorubicin, Drug resistance, Hemangiosarcoma.

Introduction

Hemangiosarcoma (HSA) is a malignant tumor in dogs (*Canis lupus familiaris*) and composed of malignant endothelial cells that are characterized by invasive growth, high metastatic rate, and poor prognosis (Withrow et al., 2013). Surgery and doxorubicin-based chemotherapy are selected as standard treatments, but several studies have described their limited efficacy (Ogilvie et al., 1996; Withrow et al., 2013). The mean survival time is 2–3 months after surgical treatment alone, and less than 1 year even

54 when chemotherapy is conducted postoperatively (Batschinski et al., 2018; Brown et al.,
55 1985). Although several improved doxorubicin-based chemotherapy protocols were
56 recently developed, they provided limited improvement of prognosis and were unable to
57 preclude tumor progression (Kahn et al., 2013; Matsuyama et al., 2017). Moreover, a
58 dose-intensified doxorubicin protocol did not show significant effects on survival time,
59 probably through acquisition of drug resistance by the tumor cells (Sorenmo et al., 2004).
60 To overcome this issue, it is essential to understand the molecular mechanisms for drug
61 resistance in HSA.

62 Chemotherapy resistance has been extensively investigated in many types of
63 cancers, and is recognized as a major cause of tumor recurrence after chemotherapy
64 (Holohan et al., 2013; Zandvliet and Teske, 2015). Several types of resistance
65 mechanisms have been reported. For example, anti-cancer drugs can be pumped out by
66 highly expressed drug efflux pumps, and genetic mutations in drug targets can prevent
67 drugs from working properly (Holohan et al., 2013). Most tumors have heterogeneity and
68 are composed of various types of tumor cells with different characteristics. This
69 heterogeneity can contribute to acquisition of drug resistance, because a particular cell
70 population with resistance to anti-cancer drugs will be selected and become dominant in
71 tumors after treatment (Burrell and Swanton, 2014; Swanton, 2012). In HSA,

72 acquisition of drug resistance after doxorubicin treatment was reported and some
73 populations had high drug efflux pump capacities (Khammanivong et al., 2016; Sorenmo
74 et al., 2000). However, the underlying mechanisms are not fully understood.

75 Most chemotherapeutic agents, including cisplatin, 5-fluorouracil, etoposide,
76 and doxorubicin, cause DNA damage, especially DNA double-strand breaks (DSBs), in
77 tumor cells (Cheung-Ong et al., 2013; Yang et al., 2015). Once DSBs are present in a cell,
78 PI3K-like serine/threonine kinases, such as ataxia telangiectasia mutated (ATM), ataxia
79 telangiectasia and Rad3 related (ATR), and DNA-dependent protein kinase (DNA-PK)
80 are activated and become localized in DNA damage sites, leading to activation of the
81 DNA damage response (DDR) pathway (Collis et al., 2005; Marechal and Zou, 2013). This
82 pathway provokes cellular senescence, cell cycle arrest, and apoptosis, and eventually
83 induces tumor cell death. DDR dysregulation was reported to contribute to drug
84 resistance (Bouwman and Jonkers, 2012; Nowsheen and Yang, 2012). For example,
85 human oral squamous cell carcinoma cells with suppressed DDR activity showed
86 resistance to cisplatin (Wang et al., 2012). However, it remains unclear whether DDR
87 dysregulation is involved in drug resistance in HSA.

88 Drug resistance is one of the major problems in HSA. To obtain better outcomes
89 after chemotherapy, it is necessary to understand the underlying molecular mechanisms

90 for drug resistance in HSA. The aims of this study were to establish doxorubicin-
91 resistant HSA cell lines and to characterize the drug-resistance mechanisms using the
92 established cell lines.
93
94 *Materials and Methods*
95 *Cell culture*
96 Two canine HSA cell lines (JuB2, Re12) were kindly given by Dr. Sakai in Gifu
97 University (Murai et al., 2012), and Human embryonic kidney 293 T cell line and HeLa
98 cell line derived from human cervical cancer were purchased from RIKEN BioResource
99 Research Center. They were cultured with Dulbecco's Modified Eagle Medium (DMEM;
100 Sigma-Aldrich, MO, USA) containing 10% fetal bovine serum (FBS; Biowest, UT, USA),
101 100 unit/ml penicillin and 100 µg/ml streptomycin (Thermo Fisher Scientific, MA, USA)
102 at 37°C with 5% CO_2. To establish doxorubicin-resistant (DR) HSA cell lines, five
103 hundred thousand cells were seeded in 10 cm cell culture dish (Falcon, NC, USA) and
104 cultured in medium containing 10 nM doxorubicin (Wako, Osaka, Japan) dissolved in
105 DMSO (Kanto Chemical Co., Inc., Tokyo, Japan) based on our previous work (Aoshima
106 et al., 2018). The medium was replaced to the fresh one every 3 days until the surviving
107 cells restarted proliferating and became 80-90% confluent. Then, the cells were passaged

(1:3) and cultured in medium containing 20 nM doxorubicin with replacing the medium to the fresh one every 3 days until the cells became 80-90% confluent. These processes were repeated with doubling doxorubicin concentration every passage timing until the cells were able to normally proliferate in a 16-fold higher doxorubicin concentration compared with the initial culture. Established cells were maintained in 160 nM doxorubicin containing medium. To inhibit drug efflux pump function, JuB2 and Re12 were exposed to 200 μM and 150 μM verapamil (Wako), a multi-pump inhibitor, respectively. These concentrations were confirmed to fully inhibit efflux of Dye Cycle Violet (DCV, Thermo Fisher Scientific) (Fig. S1).

Cell viability assay

Three thousand cells were seeded in 96 well cell culture plates (Corning, NY, USA) and were cultured with 50 μl culture medium. On the next day, they were treated with DMSO or five different concentrations (10 nM, 100 nM, 1 μM, 10 μM and 100 μM) of doxorubicin. Survival rates were analyzed using Cell Counting Kit-8 (CCK-8: Dojindo, Kumamoto, Japan) according to the manufacturer's instruction with slight modifications. Briefly, 5 μl of CCK-8 solution was added to each well 72 hours after adding DMSO or doxorubicin. After 2 hours incubation, absorbance at 450 nm was measured by Nano

126 Drop 2000 (Thermo Fisher Scientific). Survival rates were calculated by setting that of
127 DMSO treated samples as 100%. Ky Plot 5.0 software (KyensLab, Inc., Tokyo, Japan)
128 was used to draw survival curves.
129
130 *Colony formation assay*
131 Three hundred cells were seeded in 35 mm cell culture dish (FALCON) and were
132 cultured with 160 nM doxorubicin containing medium for 10 days at 37°C with 5% CO_2.
133 Then, cells were fixed with 4% paraformaldehyde (Merck-Millipore, MA, USA) for 15
134 mins at room temperature (RT). After washing with distilled water three times, cells
135 were stained with 0.01% Crystal Violet (Sigma-Aldrich) for 30 mins at RT. After washing
136 with phosphate buffered saline (PBS) and drying at RT, colonies composed of more than
137 50 cells were counted manually using an inverted microscope (Eclipse TS100; Nikon,
138 Tokyo, Japan).
139
140 *Flow cytometry*
141 Cells were detached from the cell culture dishes by 0.05% trypsin-EDTA (Wako)
142 and then filtered with 70 μm mesh filter (Grainer Bio-One, Kremsmunster, Austlia). One
143 million cells were stained with 15 μM Dye Cycle Violet (DCV, Thermo Fisher Scientific)

144 and incubated for 60 mins at 37°C with mixing the cells every 15 mins. JuB2 and Re12
145 were exposed to 200 μM and 150 μM verapamil when DCV was added to the cells.
146 Afterwards, cells were analyzed by FACS Aria II (Becton Dickinson, NJ, USA). DCV
147 efflux was measured by detecting DCV signals excited by the violet laser using 616/23
148 nm band-pass filters after excluding dead cells which were positive for 7-
149 aminoactinomycin D (Thermo Fisher Scientific) (Erdei et al., 2018).
150
151 *Alkaline Comet assay*
152 Five hundred thousand DS- and DR-HSA cells were seeded in 6 cm culture
153 dishes and cultured without doxorubicin. On the next day, cells were treated with
154 verapamil alone, or doxorubicin and verapamil. JuB2 was treated with 200 μM
155 verapamil with/without 4.6 μM doxorubicin (= the 50% growth inhibition; IC_{50}) for 30
156 mins. Re12 was treated with 150 μM verapamil with/without 0.77 μM doxorubicin (=
157 IC_{50}) for 60 mins. DMSO was used in the control. Then, the medium was replaced to the
158 fresh one without both doxorubicin and verapamil, and the cells were cultured for six
159 hours. Afterwards, the cells were detached from the dishes with 0.05% Trypsin-EDTA
160 and suspended in 1% low-melting point agarose (NIPPON GENE, Tokyo, Japan). Cell
161 suspensions containing five thousand cells were applied to MAS-coated slide glasses

(MATSUNAMI, Osaka, Japan) which were pre-coated with 1% agarose (Takara bio, Kusatsu, Japan). Slides were immersed in comet lysis buffer {1.2 M NaCl (Wako), 100 mM EDTA (Dojindo), 0.1% sodium lauryl sarcosinate (Wako), 0.26 M NaOH (Wako)} and incubated at 4°C for overnight. Then, slides were washed with alkaline rinse buffer (0.03 M NaOH, 2 mM EDTA). After DNA was separated in alkaline rinse buffer at 9 V for 15 mins, slides were washed with distilled water twice and stained with 10 μg/ml propidium iodide (Dojindo) at 4°C for 30 min. Fluorescent images were captured using an inverted fluorescence microscope (BZ-9000; KEYENCE, Osaka, Japan), and comet tails of at least 30 cells per slide were analyzed with Open Comet plugin for ImageJ software (NIH, MD, USA) (Ding et al., 2016; Gyori et al., 2014; Olive and Banath, 2006; Rasband, 1997-2018; Schneider et al., 2012).

Gamma H2A.X stain

Glass bottom dishes (MATSUNAMI, Osaka, Japan) were sterilized by exposing UV for 30 mins and coated with 0.5% bovine gelatin (Wako) for 30 mins at 37°C. Eighty thousand DS- and DR-HSA cells were seeded in the sterilized coated dishes and cultured without doxorubicin for 24 hours. Then, the cells were treated with doxorubicin/verapamil in the same way as alkaline comet assay. DMSO was used in the

control. Then, the cells were washed with PBS twice and incubated in the fresh medium without doxorubicin and verapamil at 37°C with 5% CO_2. After six hours culture, the cells were washed with PBS twice and fixed with 4% paraformaldehyde for 15 mins at RT. After washing with PBS twice, cells were permeabilized with ice-cold methanol (Wako) for 10 mins at -30°C. After washing with PBS three times and blocking with 0.3% Triton X-100 in PBS containing 1% bovine serum albumin (Sigma-Aldrich) at RT for 1 hour, the cells were incubated with gamma-H2A.X antibody (#A300-081A, 1;250, Bethyl Laboratories, TX, USA) in 0.05% Triton X-100 in PBS (PBST) overnight at 4°C. After washing with PBST twice, the cells were incubated with anti-Rabbit IgG (H+L) secondary antibody Alexa Fluor 555 (#A27039, 1:500, Thermo Fisher Scientific) and Hoechst 33342 (Thermo Fisher Scientific) at RT for 1 hour. After washing with PBST, fluorescent images were captured with a confocal microscopy (LSM-700, Carl Zeiss AG, Jena, Germany) and were processed with ImageJ software (Nikolova et al., 2014; Rasband, 1997-2018; Schneider et al., 2012).

Protein extraction and western blotting

Samples were prepared, separated and transferred to PVDF membranes as described previously (Aoshima et al., 2018). Membranes were either incubated with anti-

198 ABCB1 antibody (#ab170904, 1:2,500, abcam, Cambridge, UK), anti-ABCG2 antibody
199 (#ab3380, 1:1,000, abcam), anti-ATM antibody (#NB100-104, 1:1,000, Novus biologicals,
200 CO, USA), anti-cleaved caspase-3 (Asp175) antibody (#9661, 1:1,000, Cell signaling, MA,
201 USA) (Penzo-Méndez et al. 2015) or anti-actin antibody clone C4 (#MAB1501, 1:10,000,
202 Merck Millipore) for overnight at 4°C. After washing with Tris-buffered saline containing
203 0.05% Tween 20 (TBST), membranes were incubated with ECL rabbit IgG HRP-linked
204 whole Ab (#NA934-1ML, 1:10,000, GE Healthcare, IL, USA) or ECL mouse IgG HRP-
205 linked whole Ab (#NA931-1ML, 1:10,000, GE Healthcare) for 1 hour at RT. After washing
206 with TBST, signals were developed with Immobilon Western Chemiluminescent HRP
207 substrate (Merck Millipore) and detected by ImageQuant LAS 4000 mini (GE
208 Healthcare). Signal intensities were obtained by ImageJ software (Rasband, 1997-2018;
209 Schneider et al., 2012). Expression levels of ATM and cleaved caspase-3 were normalized
210 with actin expression levels.
211
212 *RNA extraction and reverse transcription quantitative polymerase chain reaction (RT-*
213 *qPCR)*
214 Primers and samples were prepared as described previously (Aoshima et al.,
215 2018). qPCR was performed using the primers listed in Table 1. Results were normalized

based on the geometric mean of reference genes (*ACTB, HMBS, RPLL3A* and *TBP*), which were selected from 9 potential internal controls (*GAPDH, ACTB, B2M, HMBS, HPRT1, RPLL3A, RPL32, TBP* and *YWHAZ*) by geNorm software (Fig. S2) (Peters et al., 2007; Vandesompele et al., 2002). Relative expression levels were calculated by setting the DS-HSA cell lines as the control.

Statistical Analysis

Levels of significance were determined by Mann-Whitney U test, Student's *t* test or Dunnet's test. *p* values lower than 0.05 were considered statistically significant.

Results

Establishment of doxorubicin-resistant canine hemangiosarcoma cell lines

To confirm that the established DR-HSA cells had truly attained resistance to doxorubicin, they were treated with various concentrations of doxorubicin for 72 h and analyzed for their survival rates to create survival curves. Comparisons of these survival curves with those of parental doxorubicin-sensitive (DS) HSA cells revealed that DR-HSA cells were able to survive under higher doxorubicin concentrations than DS-HSA cells (Fig. 1a top). IC_{50} values of DR-HSA cells were higher than those of DS-HSA cells

234 (Fig. 1a bottom). Colony formation assay was performed to investigate the proliferation
235 in the presence of high concentrations of doxorubicin (160 nM). DR-HSA cells were able
236 to form larger numbers of colonies than DS-HSA cells (Fig. 1b). These results indicated
237 that DR-HSA cell lines were successfully generated.
238
239 *DR-HSA cells have higher efflux pump capacity than DS-HSA cells.*
240 High drug efflux pump capacity was previously determined to be an important
241 factor for acquisition of drug resistance, because it enables tumor cells to pump out anti-
242 cancer drugs (Gottesman et al. 2002). To measure the drug efflux pump activities in DR-
243 HSA cells, cells were stained with DCV, a cell-permeable DNA dye that can be excreted
244 by drug efflux pumps, with or without verapamil, a multi-drug pump inhibitor.
245 Comparing the percentages of DCV negative population of DR-HSA and DS-HSA cells
246 clearly indicated that DR-HSA cells had higher drug efflux pump capacity than DS-HSA
247 cells in both JuB2 and Re12 cells, even though the percentages of DCV negative
248 population were different between JuB2 and Re12 (Fig. 2a). Next, we analyzed gene and
249 protein expression levels of major ATP-binding cassette (ABC) transporters to determine
250 which drug pump is responsible for this phenotype. Although no ABC transporter was
251 upregulated in DR-HSA cells at the mRNA level (Fig. 2b), ABCB1 and ABCG2 were

252 significantly upregulated in DR-HSA cells at the protein level (Fig. 2c). To further
253 confirm that the high efflux pump capacity was responsible for doxorubicin resistance in
254 HSA cells, we analyzed the survival rates of DR- and DS-HSA cells after 24h treatment
255 with ABC transporter inhibitor, verapamil, with or without 160 nM doxorubicin. The
256 viability of cells treated with verapamil alone for 24h was quite low because verapamil
257 *per se* exerts toxic effects on cell viability by disrupting the calcium balance in cells (Zhao
258 et al., 2016). Cell viability of DR-JuB2 cells, however, was the same as that of DS-JuB2
259 cells under doxorubicin and verapamil treatments, suggesting that drug efflux pump
260 inhibition by verapamil treatment may reverse doxorubicin sensitivity in DR-JuB2 cells
261 (Fig. 2d). These results suggest that high efflux pump capacity contributes to doxorubicin
262 resistance, especially in JuB2 cells.
263
264 *DNA damage response in DR-HSA cells is weaker than that in DS-HSA cells*
265 Doxorubicin could be pumped out of some DR-HSA cells based on the above
266 results, while other cells remained DCV-positive despite their normal proliferation in the
267 presence of doxorubicin (Fig. 1a, 2a). In DR-Re12 cells in particular, approximately 90%
268 of cells were not defined as the DCV negative population, suggesting that other functions
269 are involved in the acquisition of doxorubicin resistance in HSA cells. Because

doxorubicin-induced cell death is mainly provoked by DNA damage through DSBs (Yang et al., 2015; Yang et al., 2014), two hypotheses were conceived. The first was that DNA in DR-HSA cells received less damage by doxorubicin than that in DS-HSA cells, and the second was that the DDR did not work effectively in DR-HSA cells and they were unable to induce apoptosis.

To address the first hypothesis, we evaluated DNA damage by alkaline comet assays (Ding et al., 2016; Olive and Banath, 2006). To compare the effects of doxorubicin on DNA damage between DS-HSA and DR-HSA cells, verapamil was added with doxorubicin to eliminate any discrepancy caused by the drug efflux pump capacities. After treatment with the drugs, JuB2 and Re12 cells were cultured with fresh medium without drugs for more 6 h, and their tail percentages were calculated as indicators of DNA damage at specific time points. DNA damage was significantly accumulated in the doxorubicin-treated groups compared with the control groups in all cells except for DR-Re12 cells, and the DNA damage was not affected by verapamil treatment alone (Fig. 3a and c). Interestingly, accumulation of DNA damage did not differ significantly between DR-JuB2 and DS-JuB2 cells (Fig. 3b), while DR-Re12 cells accumulated DNA damage even before addition of doxorubicin, the degree of which was close to that in DS-Re12 cells after 6 h of doxorubicin treatment (Fig. 3c and d). In both cell lines, sooner or later,

288 DR-HSA cells accumulated DNA damage to a similar or greater extent than DS-HSA
289 cells after doxorubicin treatment.

290 Next, we addressed the second hypothesis. To examine whether the DDR was
291 induced by doxorubicin, γH2A.X signals were investigated. γH2A.X is widely used as a
292 biomarker for DSBs because it accumulates at DSB sites to promote repair of the damage
293 by the DDR (Nikolova et al., 2014). We used an anti-human γH2A.X antibody, which was
294 confirmed to cross-react to canine γH2A.X (Fig. S3a). Verapamil was added with
295 doxorubicin to eliminate the differences in high efflux pump capacity between DS-HSA
296 and DR-HSA cells. After γH2A.X staining, the mean number of γH2A.X foci/cell in DR-
297 HSA cells was significantly lower than that in DS-HSA cells (Fig. 4), suggesting that the
298 DDR was repressed in DR-HSA cells compared with DS-HSA cells. DDR-related genes
299 were also downregulated in DR-HSA cells (Fig. 5a). Protein expression of ATM, a major
300 DDR factor protein, was analyzed using an anti-human ATM antibody. The antibody was
301 confirmed to cross-react canine ATM (Fig. S3b) and showed that ATM protein expression
302 was significantly downregulated in DR-HSA cells (Fig. 5b).

303 To further validate that the DDR was repressed in DR-HSA cells, we
304 investigated the apoptotic activity in the cell lines by analyzing cleaved caspase-3
305 expression after verapamil treatment with or without doxorubicin. Cleaved caspase-3

306 was detected after treatment in both DR-HSA and DS-HSA cells, but DR-HSA cells
307 showed much lower expression than DS-HSA cells (Fig. 5c). These results suggested that
308 apoptosis was less activated in DR-HSA cells compared with DS-HSA cells.
309 The above findings indicated that the DDR was repressed in DR-HSA cells
310 despite their accumulation of DNA damage, suggesting that DR-HSA cells avoided
311 apoptosis and acquired resistance to doxorubicin.
312
313 *Discussion*
314 High drug efflux pump capacity has been recognized as one of the major drug-
315 resistance mechanisms in tumors (Zandvliet and Teske, 2015). Likewise, in the present
316 study, DR-HSA cells exhibited higher DCV negative population percentages than DS-
317 HSA cells. Interestingly, the DCV negative population percentages also differed between
318 JuB2 and Re12 cells. Specifically, approximately 65% of DR-JuB2 cells were identified
319 as the DCV negative population, compared with only 9% of DR-Re12 cells. Furthermore,
320 verapamil treatment reversed doxorubicin sensitivity in JuB2 but not in Re12 cells. This
321 difference implies that high drug efflux pump capacity is related to doxorubicin
322 resistance but is not always a major drug resistance mechanism in HSA. The IC_{50} value
323 of JuB2 cells was approximately 5–6 times higher than that of Re12 cells. This

discrepancy probably arose by the different drug efflux pump capacities, because a much higher percentage of JuB2 cells were identified in the DCV negative population compared with Re12 cells. ABCB1 and ABCG2 protein expression was upregulated in DR-HSA cells compared with DS-HSA cells. The mRNA expression of these genes and some other ABC transporters, however, was not enhanced in DR-HSA cells. This discrepancy could be explained by the suppression of the ubiquitin-proteasome degradation pathway (Katayama et al., 2016), translational efficiency, or a difference in the half lives of mRNA and protein (Day and Tuite, 1998; Haenisch et al., 2007; Petriz et al., 2004). Another possibility for the differences between JuB2 and Re12 may be related to tumor heterogeneity. Some specific populations could be selected by long-term cell culture to establish the cell lines, which may have endowed different features on each cell line. The tumor origins may also be responsible because JuB2 cells originated from a hepatic HSA, while Re12 cells originated from a cardiac HSA. It was reported that endothelial cells are heterogeneous and possess organ-specific phenotypes (Marcu et al., 2018; Rafii et al., 2016). Thus, it is possible that canine HSA cells have different phenotypes based on their origins, and further research is required to address this issue.

We also found that the DDR was repressed in DR-HSA cells despite their high DNA damage burdens by doxorubicin, leading to doxorubicin resistance probably by

342 circumventing apoptosis. Apoptosis evasion is well known as a hallmark of cancer cells
343 (Fouad and Aanei, 2017). It can be established by several mechanisms, including DNA
344 damage unresponsiveness, mutations in anti-apoptotic genes, and posttranslational
345 deregulation of pro-apoptotic genes (Fernald and Kurokawa, 2013). In the present study,
346 γH2A.X signals were not significantly increased in both DR-HSA cell lines after
347 doxorubicin treatment. Furthermore, the gene and protein expression levels of DDR
348 factors were significantly decreased in the DR-HSA cell lines. It was reported that ATM
349 expression can be repressed by micro RNA in human breast cancers and colorectal
350 cancers (Song et al., 2011; Zhou et al., 2014), but the detailed mechanism in HSA remains
351 unclear. Moreover, cleaved caspase 3 induction by verapamil treatment alone (V+/D−)
352 was weak in DR-HSA cells compared with DS-HSA cells. Verapamil treatment did not
353 affect the DNA damage burden, suggesting that other mechanisms unrelated to the DDR
354 lead to apoptosis evasion in DR-HSA cells. However, doxorubicin has been reported to
355 induce apoptosis in DNA damage-independent manner (Gewirtz, 1999; Swift et al., 2006),
356 so further studies are required to reveal the mechanisms completely.

357 In this study, DR-JuB2 and DR-Re12 cells reacted differently to doxorubicin
358 treatment. DR-JuB2 cells received DNA damage in the same way as DS-JuB2 cells, while
359 DR-Re12 cells accumulated significantly more DNA damage than DS-Re12 cells even

360 before doxorubicin treatment. This difference probably arose through the number of cells
361 with high drug efflux pump capacity in the population, *i.e.* JuB2 cells mainly relied on
362 drug efflux to circumvent the harmful effects of doxorubicin. Meanwhile, in DR-Re12
363 cells, the weak DDR was probably more important than drug efflux, because most DR-
364 Re12 cells did not have high drug efflux pump capacity and showed less ATM expression
365 and distinctly lower apoptosis induction than DR-JuB2 cells. Verapamil treatment alone
366 induced more cell death in DR-Re12 compared with DS-Re12, which might be explained
367 by other verapamil toxicities such as autophagy-like processes in apoptosis-resistant
368 cells (Pajak et al., 2012). There was no significant difference in the tail DNA percentages
369 with and without doxorubicin in DR-Re12 cells. This may have arisen because the assay
370 condition in the present study was unable to detect very high DNA damage, *i.e.* the
371 signals were saturated. Tumor cells with high DNA damage burdens and apoptosis-
372 evasion capability will accumulate DNA mutations in their genome followed by
373 increasing genome instability (Lord and Ashworth, 2012). This can lead to genome
374 amplification or deletion, which may result in cell cycle dysregulation, acquisition of
375 invasiveness and metastatic ability as well as resistance against fatal DNA damage
376 (Squatrito et al., 2010; Yao and Dai, 2014; Zhivotovsky and Kroemer, 2004). To greater
377 or lesser extents, both cell lines in the present study acquired resistance to doxorubicin

by evading apoptosis. Further characterization of DR-HSA cells should be conducted to reveal whether doxorubicin resistance in HSA cells bestows more malignant features on the cells.

In conclusion, we have established doxorubicin-resistant canine HSA cell lines and indicated that high DNA efflux pump capacity and low DNA damage responses are part of their resistance mechanisms. Angiosarcoma, a human counterpart of HSA, has similar characteristics to canine HSA and also has no effective treatment (Young et al., 2010). Because human angiosarcoma is a very rare tumor, canine HSA has attracted attention as a good animal model for understanding its pathogenesis (Fosmire et al., 2004). Although further research using experimental animal models and clinical cases is required to fully elucidate the mechanism for chemotherapy resistance in HSA, the present findings provide a stepping stone to promote drug resistance studies in HSA as well as human angiosarcoma.

Conflict of interest

The authors declare that they have no conflicts of interest with the contents of this article.

References

Aoshima, K., Fukui, Y., Gulay, K.C.M., Erdemsurakh, O., Morita, A., Kobayashi, A., Kimura, T., 2018. Notch2 signal is required for the maintenance of canine hemangiosarcoma cancer stem cell-like cells. BMC Vet Res 14, 301.

Batschinski, K., Nobre, A., Vargas-Mendez, E., Tedardi, M.V., Cirillo, J., Cestari, G., Ubukata, R., Dagli, M.L.Z., 2018. Canine visceral hemangiosarcoma treated with surgery alone or surgery and doxorubicin: 37 cases (2005-2014). Can Vet J 59, 967-972.

Bouwman, P., Jonkers, J., 2012. The effects of deregulated DNA damage signalling on cancer chemotherapy response and resistance. Nat Rev Cancer 12, 587-598.

Brown, N.O., Patnaik, A.K., MacEwen, E.G., 1985. Canine hemangiosarcoma: retrospective analysis of 104 cases. J Am Vet Med Assoc 186, 56-58.

Burrell, R.A., Swanton, C., 2014. Tumour heterogeneity and the evolution of polyclonal drug resistance. Mol Oncol 8, 1095-1111.

Cheung-Ong, K., Giaever, G., Nislow, C., 2013. DNA-damaging agents in cancer chemotherapy: serendipity and chemical biology. Chem Biol 20, 648-659.

Collis, S.J., DeWeese, T.L., Jeggo, P.A., Parker, A.R., 2005. The life and death of DNA-PK. Oncogene 24, 949-961.

Day, D.A., Tuite, M.F., 1998. Post-transcriptional gene regulatory mechanisms in eukaryotes: an overview. J Endocrinol 157, 361-371.

Ding, W., Bishop, M.E., Lyn-Cook, L.E., Davis, K.J., Manjanatha, M.G., 2016. In Vivo Alkaline Comet Assay and Enzyme-modified Alkaline Comet Assay for Measuring DNA Strand Breaks and Oxidative DNA Damage in Rat Liver. J Vis Exp.

Erdei, Z., Schamberger, A., Torok, G., Szebenyi, K., Varady, G., Orban, T.I., Homolya, L., Sarkadi, B., Apati, A., 2018. Generation of multidrug resistant human tissues by overexpression of the ABCG2 multidrug transporter in embryonic stem cells. PLoS One 13, e0194925.

Fernald, K., Kurokawa, M., 2013. Evading apoptosis in cancer. Trends Cell Biol 23, 620-633.

Fosmire, S.P., Dickerson, E.B., Scott, A.M., Bianco, S.R., Pettengill, M.J., Meylemans, H., Padilla, M., Frazer-Abel, A.A., Akhtar, N., Getzy, D.M., Wojcieszyn, J., Breen, M., Helfand, S.C., Modiano, J.F., 2004. Canine malignant hemangiosarcoma as a model of primitive angiogenic endothelium. Laboratory Investigation 84, 562-572.

Fouad, Y.A., Aanei, C., 2017. Revisiting the hallmarks of cancer. American Journal of Cancer Research 7, 1016-1036.

Gewirtz, D.A., 1999. A critical evaluation of the mechanisms of action proposed for the antitumor effects of the anthracycline antibiotics Adriamycin and daunorubicin. Biochemical Pharmacology 57, 727-741.

Gyori, B.M., Venkatachalam, G., Thiagarajan, P.S., Hsu, D., Clement, M.V., 2014.

OpenComet: an automated tool for comet assay image analysis. Redox Biol 2, 457-465.
Haenisch, S., Zimmermann, U., Dazert, E., Wruck, C.J., Dazert, P., Siegmund, W., Kroemer, H.K., Warzok, R.W., Cascorbi, I., 2007. Influence of polymorphisms of ABCB1 and ABCC2 on mRNA and protein expression in normal and cancerous kidney cortex. Pharmacogenomics J 7, 56-65.
Holohan, C., Van Schaeybroeck, S., Longley, D.B., Johnston, P.G., 2013. Cancer drug resistance: an evolving paradigm. Nat Rev Cancer 13, 714-726.
Kahn, S.A., Mullin, C.M., de Lorimier, L.P., Burgess, K.E., Risbon, R.E., Fred, R.M., 3rd, Drobatz, K., Clifford, C.A., 2013. Doxorubicin and deracoxib adjuvant therapy for canine splenic hemangiosarcoma: a pilot study. Can Vet J 54, 237-242.
Katayama, K., Fujiwara, C., Noguchi, K., Sugimoto, Y., 2016. RSK1 protects P-glycoprotein/ABCB1 against ubiquitin-proteasomal degradation by downregulating the ubiquitin-conjugating enzyme E2 R1. Sci Rep 6, 36134.
Khammanivong, A., Gorden, B.H., Frantz, A.M., Graef, A.J., Dickerson, E.B., 2016. Identification of drug-resistant subpopulations in canine hemangiosarcoma. Vet Comp Oncol 14, e113-125.
Lord, C.J., Ashworth, A., 2012. The DNA damage response and cancer therapy. Nature 481, 287-294.
Marcu, R., Choi, Y.J., Xue, J., Fortin, C.L., Wang, Y., Nagao, R.J., Xu, J., MacDonald, J.W., Bammler, T.K., Murry, C.E., Muczynski, K., Stevens, K.R., Himmelfarb, J., Schwartz, S.M., Zheng, Y., 2018. Human Organ-Specific Endothelial Cell Heterogeneity. iScience 4, 20-35.
Marechal, A., Zou, L., 2013. DNA damage sensing by the ATM and ATR kinases. Cold Spring Harb Perspect Biol 5.
Matsuyama, A., Poirier, V.J., Mantovani, F., Foster, R.A., Mutsaers, A.J., 2017. Adjuvant Doxorubicin with or without Metronomic Cyclophosphamide for Canine Splenic Hemangiosarcoma. Journal of the American Animal Hospital Association 53, 304-312.
Murai, A., Abou Asa, S., Kodama, A., Hirata, A., Yanai, T., Sakai, H., 2012. Constitutive phosphorylation of the mTORC2/Akt/4E-BP1 pathway in newly derived canine hemangiosarcoma cell lines. Bmc Veterinary Research 8.
Nikolova, T., Dvorak, M., Jung, F., Adam, I., Kramer, E., Gerhold-Ay, A., Kaina, B., 2014. The gammaH2AX assay for genotoxic and nongenotoxic agents: comparison of H2AX phosphorylation with cell death response. Toxicol Sci 140, 103-117.
Nowsheen, S., Yang, E.S., 2012. The intersection between DNA damage response and cell death pathways. Exp Oncol 34, 243-254.
Ogilvie, G.K., Powers, B.E., Mallinckrodt, C.H., Withrow, S.J., 1996. Surgery and doxorubicin in dogs with hemangiosarcoma. J Vet Intern Med 10, 379-384.

468 Olive, P.L., Banath, J.P., 2006. The comet assay: a method to measure DNA damage in
469 individual cells. Nat Protoc 1, 23-29.
470 Pajak, B., Kania, E., Gajkowska, B., Orzechowski, A., 2012. Verapamil-induced autophagy-
471 like process in colon adenocarcinoma COLO 205 cells; the ultrastructural studies. Pharmacol
472 Rep 64, 991-996.
473 Peters, I.R., Peeters, D., Helps, C.R., Day, M.J., 2007. Development and application of
474 multiple internal reference (housekeeper) gene assays for accurate normalisation of canine
475 gene expression studies. Vet Immunol Immunopathol 117, 55-66.
476 Petriz, J., Gottesman, M.M., Aran, J.M., 2004. An MDR-EGFP gene fusion allows for direct
477 cellular localization, function and stability assessment of P-glycoprotein. Curr Drug Deliv 1,
478 43-56.
479 Rafii, S., Butler, J.M., Ding, B.S., 2016. Angiocrine functions of organ-specific endothelial
480 cells. Nature 529, 316-325.
481 Rasband, W.S., 1997-2018. ImageJ, U. S. . National Institutes of Health.
482 Schneider, C.A., Rasband, W.S., Eliceiri, K.W., 2012. NIH Image to ImageJ: 25 years of image
483 analysis. Nat Methods 9, 671-675.
484 Song, L.B., Lin, C.Y., Wu, Z.Q., Gong, H., Zeng, Y., Wu, J.H., Li, M.F., Li, J., 2011. miR-18a
485 Impairs DNA Damage Response through Downregulation of Ataxia Telangiectasia Mutated
486 (ATM) Kinase. Plos One 6.
487 Sorenmo, K., Duda, L., Barber, L., Cronin, K., Sammarco, C., Usborne, A., Goldschmidt, M.,
488 Shofer, F., 2000. Canine hemangiosarcoma treated with standard chemotherapy and
489 minocycline. Journal of Veterinary Internal Medicine 14, 395-398.
490 Sorenmo, K.U., Baez, J.L., Clifford, C.A., Mauldin, E., Overley, B., Skorupski, K., Bachman,
491 R., Samluk, M., Shofer, F., 2004. Efficacy and toxicity of a dose-intensified doxorubicin
492 protocol in canine hemangiosarcoma. Journal of Veterinary Internal Medicine 18, 209-213.
493 Squatrito, M., Brennan, C.W., Helmy, K., Huse, J.T., Petrini, J.H., Holland, E.C., 2010. Loss
494 of ATM/Chk2/p53 Pathway Components Accelerates Tumor Development and Contributes to
495 Radiation Resistance in Gliomas. Cancer Cell 18, 619-629.
496 Swanton, C., 2012. Intratumor Heterogeneity: Evolution through Space and Time. Cancer
497 Research 72, 4875-4882.
498 Swift, L.P., Rephaeli, A., Nudelman, A., Phillips, D.R., Cutts, S.M., 2006. Doxorubicin-DNA
499 adducts induce a non-topoisomerase II-mediated form of cell death. Cancer Research 66,
500 4863-4871.
501 Vandesompele, J., De Preter, K., Pattyn, F., Poppe, B., Van Roy, N., De Paepe, A., Speleman,
502 F., 2002. Accurate normalization of real-time quantitative RT-PCR data by geometric
503 averaging of multiple internal control genes. Genome Biol 3, RESEARCH0034.

Wang, L., Mosel, A.J., Oakley, G.G., Peng, A.M., 2012. Deficient DNA Damage Signaling Leads to Chemoresistance to Cisplatin in Oral Cancer. Molecular Cancer Therapeutics 11, 2401-2409.

Withrow, S.J., Vail, D.M., Page, R.L., 2013. Withrow & MacEwen's small animal clinical oncology, 5th ed. Elsevier, St. Louis, Mo.

Yang, F., Kemp, C.J., Henikoff, S., 2015. Anthracyclines induce double-strand DNA breaks at active gene promoters. Mutation Research-Fundamental and Molecular Mechanisms of Mutagenesis 773, 9-15.

Yang, F., Teves, S.S., Kemp, C.J., Henikoff, S., 2014. Doxorubicin, DNA torsion, and chromatin dynamics. Biochimica Et Biophysica Acta-Reviews on Cancer 1845, 84-89.

Yao, Y., Dai, W., 2014. Genomic Instability and Cancer. J Carcinog Mutagen 5.

Young, R.J., Brown, N.J., Reed, M.W., Hughes, D., Wall, P.J., 2010. Angiosarcoma. Lancet Oncology 11, 983-991.

Zandvliet, M., Teske, E., 2015. Mechanisms of Drug Resistance in Veterinary Oncology- A Review with an Emphasis on Canine Lymphoma. Vet Sci 2, 150-184.

Zhao, L., Zhao, Y., Schwarz, B., Mysliwietz, J., Hartig, R., Camaj, P., Bao, Q., Jauch, K.W., Guba, M., Ellwart, J.W., Nelson, P.J., Bruns, C.J., 2016. Verapamil inhibits tumor progression of chemotherapy-resistant pancreatic cancer side population cells. Int J Oncol 49, 99-110.

Zhivotovsky, B., Kroemer, G., 2004. Apoptosis and genomic instability. Nat Rev Mol Cell Biol 5, 752-762.

Zhou, Y., Wan, G., Spizzo, R., Ivan, C., Mathur, R., Hu, X., Ye, X., Lu, J., Fan, F., Xia, L., Calin, G.A., Ellis, L.M., Lu, X., 2014. miR-203 induces oxaliplatin resistance in colorectal cancer cells by negatively regulating ATM kinase. Mol Oncol 8, 83-92.

533

534

535 Figure legends

536 Fig.1 Establishment of DR-HSA cell lines.

537 (a) (Top) Survival curves of DR- and DS-HSA cells under doxorubicin treatment. *p*-value

538 was calculated with Mann-Whitney U test. All samples were analyzed in triplicate.

539 Survival curves are plotted as average percentages ± SD. Survival curves were calculated

540 using the following equations by least-squares method using Ky Plot 5.0 software based

541 on the results of cell viability assay. DS- JuB2: $y=4.4\times10^{-4}/(x+4.2\times10^{-6})$, DR-JuB2:

542 $y=2.7\times10^{-3}/(x+2.9\times10^{-5})$, DS-Re12: $y=6.7\times10^{-5}/(x+5.8\times10^{-7})$, DR-Re12: $y=4.5\times10^{-4}/(x+3.9\times10^{-6})$. y=survival rate (%), x=doxorubicin concentration (M). (Bottom) IC_{50}s of

544 DR and DS-HSA cell lines. (b) Colony formation assay for DR- and DS-HSA cells. $^{**}P$

545 <0.01. Student's *t* test. All samples were analyzed in triplicate and the scores are

546 presented as means ±SD.

547

548 Fig. 2 DR-HSA cells have higher drug efflux pump capacity than DR-HSA cells.

549 (a) (Left) Flow cytometry analysis to analyze DCV efflux capacity. DCV− = DCV

550 negative population. All samples were analyzed in triplicate. (Right) Quantitative

551 analysis of the DCV negative populations in each cell line. **P<0.01. Student's t test.
552 The percentages of the DCV negative populations are presented as average percentages
553 ± SD. (b) Gene expression profiles of ABC transporters. All samples were analyzed in
554 triplicate and the scores are presented as means ± SD. (c) Representative images of
555 western blotting and quantitative data analysis for ABCB1 (top) and for ABCG2 (bottom).
556 293T (Dox 24h) is a protein sample from 293T cells treated with doxorubicin for 24h and
557 was used as the positive control for both antibodies. *P<0.05. **P< 0.01. Student's t test.
558 All samples were analyzed in triplicate. The scores are presented as means ± SD. (d)
559 Survival rate of DR- and DS-HSA cell lines after 24h treatment of verapamil with or
560 without doxorubicin (V+/D– and V+/D+, respectively). *P<0.05. **P<0.01. Student's t
561 test. All samples were analyzed in triplicate. The scores are presented as means ± SD.
562

563 Fig. 3 DR-HSA cells have similar amounts of DNA damage burden to DS-HSA cells
564 after doxorubicin treatment.

565 (a, c) Alkaline comet assay for DR- and DS-HSA cells treated with verapamil (V) and
566 with/without doxorubicin (D). V+/D+ (0h) indicates the groups analyzed
567 immediately after adding drugs. V+/D– (6h) and V+/D+ (6h) indicate the groups
568 analyzed after drug treatments followed by -6h culture without doxorubicin and

569 verapamil. V−/D− (0h) indicates the control group cultured with DMSO. DNA damage
570 burdens were analyzed by percentages of DNA in the tails (Tail DNA%) calculated
571 using Open Comet plugin for imageJ software. *P<0.05, **P<0.01. Dunnet's test. All
572 samples were analyzed in triplicate and Tail DNA% are present as means ± SD. (b, d)
573 Combined graphs of (a) and (c), respectively, to compare DNA damage burdens
574 between DS- and DR- HSA cells in each condition. *P<0.05, **P<0.01. Student's t
575 test.
576
577 Fig. 4 DNA damage response is repressed in DR-HSA cells.
578 (a, c) Representative images of γH2A.X staining for DR- and DS-HSA cells treated with
579 verapamil (V) and with/without doxorubicin (D). (b, d) The number of γH2A.X signal foci
580 was calculated by imageJ software. **P<0.01. Student's t test. Bars = 10 μm. All samples
581 were analyzed in triplicate. Scores are presented as means ± SD.
582
583 Fig. 5 DDR is repressed in DR-HSA cells.
584 (a) Gene expression levels of DDR factors were evaluated by qPCR. The gene
585 expression levels in DS-HSA cells were set to 1 in each cell line. **P<0.01. Student's t
586 test. All samples were analyzed in triplicate and the scores are presented as means ±

587 SD. (b) Representative images of western blotting for ATM and quantitative data

588 analysis for ATM protein expression levels. *P<0.05. Student's t test. All samples were

589 analyzed in triplicate. The scores are presented as means ± SD. (c) Representative images

590 of western blotting and quantitative data analysis for cleaved-caspase3 after 12h (JuB2)

591 and 24h (Re12) culture with verapamil (V) and with/without doxorubicin (D).The

592 concentrations of verapamil and doxorubicin were the same as those in alkaline comet

593 assay. *p <0.05. Student's t test. All samples were analyzed in triplicates. The scores

594 are presented as means ± SD.

595 Fig. S1

596 (Top) Flow cytometry analysis to confirm that verapamil functions to inhibit DCV

597 efflux in HSA cell lines. These graphs compared the DCV negative population between

598 DR- and DS-cells in each cell line under verapamil treatment conditions. Original data

599 are shown in Figure 2a. DCV− = DCV negative population. All samples were analyzed

600 in triplicate. (Bottom) Quantitative analysis of the DCV negative populations in each

601 cell line. Student's t test. The percentages of the DCV negative populations are

602 presented as average percentages ± SD.

603

604 Fig. S2

605 Results of geNorm analysis for reference gene candidates. To determine optimal

606 number of reference genes, 0.15 V value was used as the cut-off value (Vandesompele et

607 al. 2002).

608

609

610 Fig. S3

611 Western blot analysis for (a) γ H2A.X and (b) ATM. 293T cells and HeLa cells were used

612 as the positive controls.

613

Author contributions

AM and KA designed and conceived the experiments. AM, KG, YS and HY performed the experiments and analyzed the corresponding results. AM and KA wrote the paper. HY, AK and TK revised the paper critically for important intellectual content. All authors read and approved the final manuscript.

Acknowledgements

We would like to extend our sincerest gratitude to Dr. Hiroki Sakai (Gifu University) for providing canine hemangiosarcoma cell lines. We also acknowledge the efforts of Dr. Soichiro Yamaguchi and Dr. Jumpei Yamazaki, Faculty of Veterinary Medicine, Hokkaido University for giving useful pieces of advice and constructive discussion. We are grateful to all the members of Laboratory of Comparative Pathology and Laboratory of Radiation Biology, Faculty of Veterinary Medicine, Hokkaido University for their helpful discussions, encouragements, and support. This research was supported by JSPS KAKENHI Grant-in-Aid for Young Scientist (KA, Number 18K14575). Finally, we thank H. Nikki March, PhD, from Edanz Group (www.edanzediting.com/ac for editing a draft of this manuscript.

a

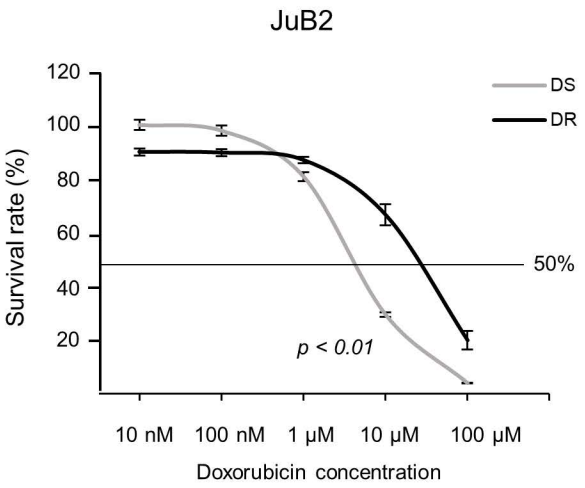

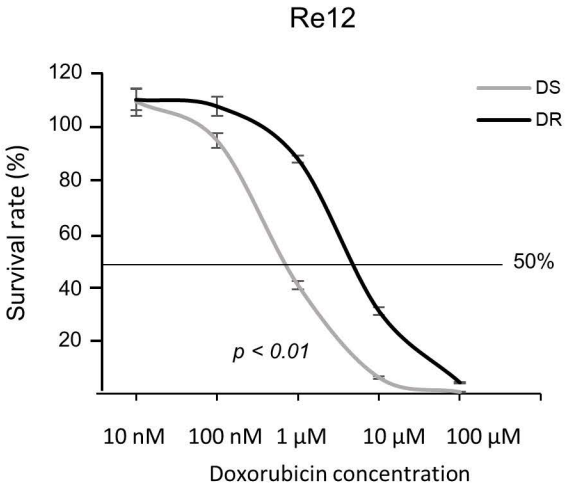

IC50 (DS-JuB2)	4.6 (± 0.23) μM
IC50 (DR-JuB2)	25.6 (± 5.5) μM

IC50 (DS-Re12)	0.77 (± 0.04) μM
IC50 (DR-Re12)	5.1 (± 0.27) μM

b

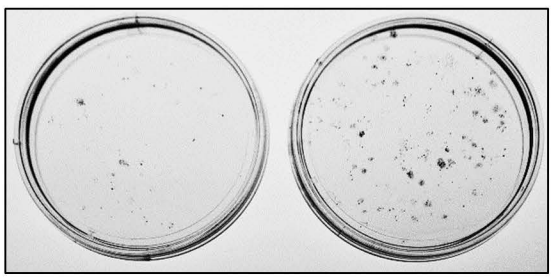

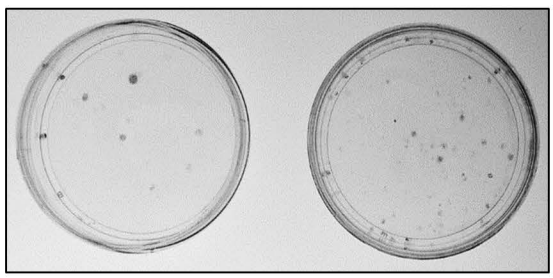

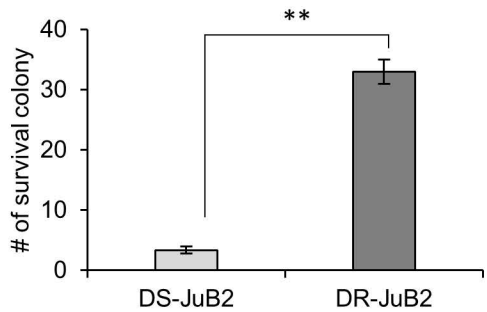

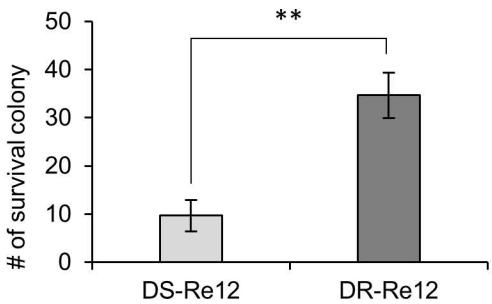

Fig. 1 Morita *et al.*

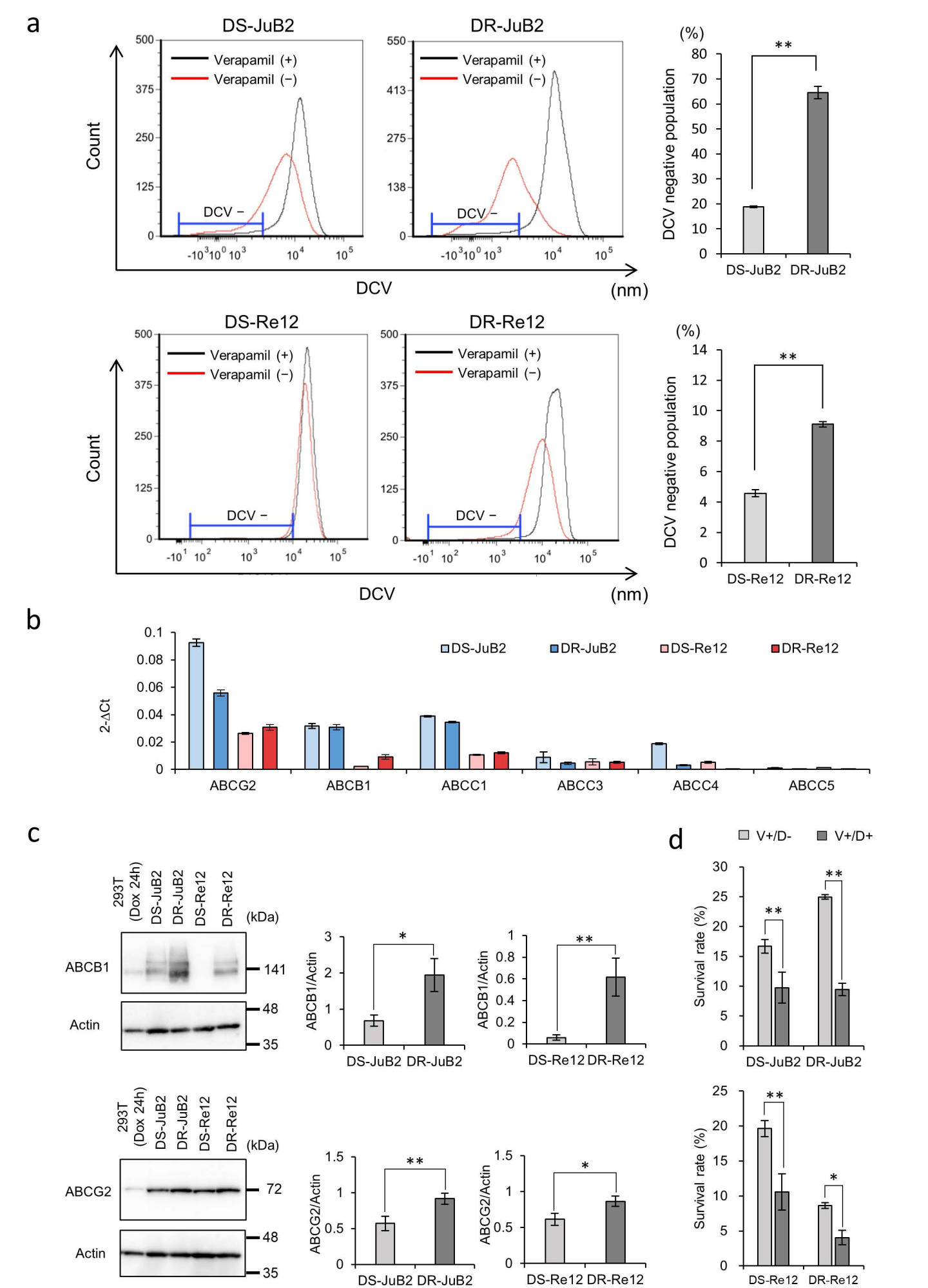

Fig. 2 Morita *et al.*

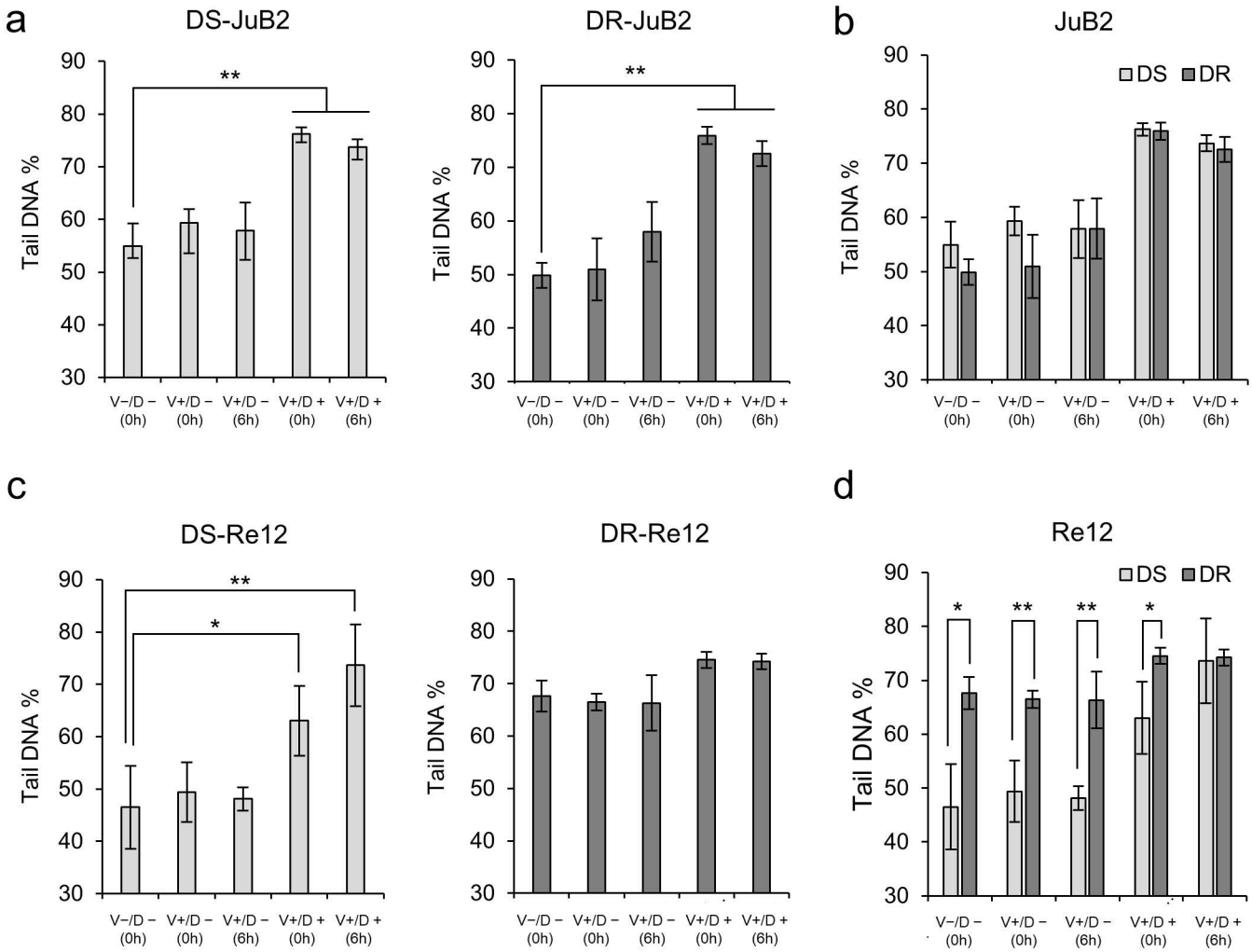

Fig. 3 Morita *et al.*

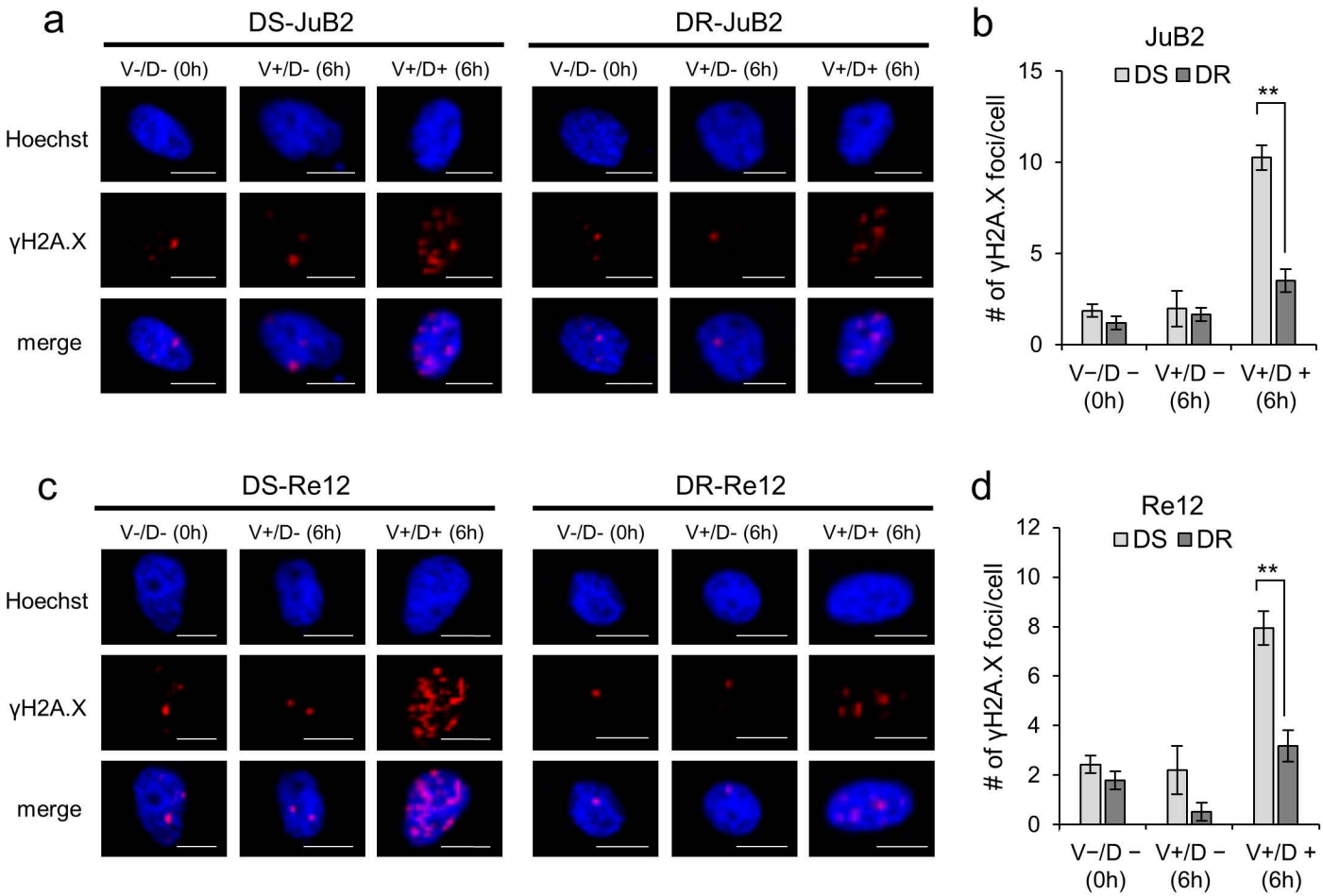

Fig. 4 Morita *et al.*

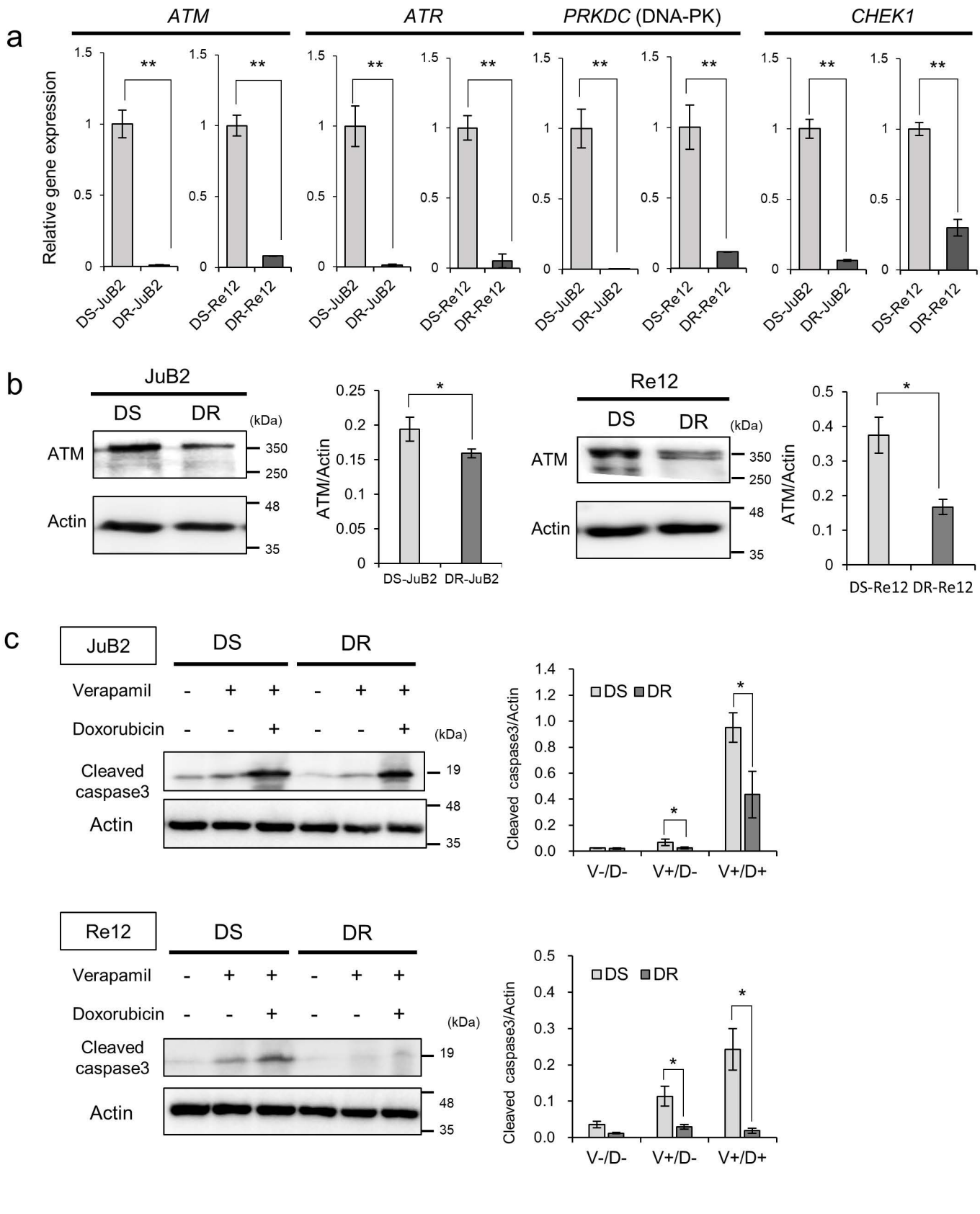

Fig. 5 Morita *et al.*

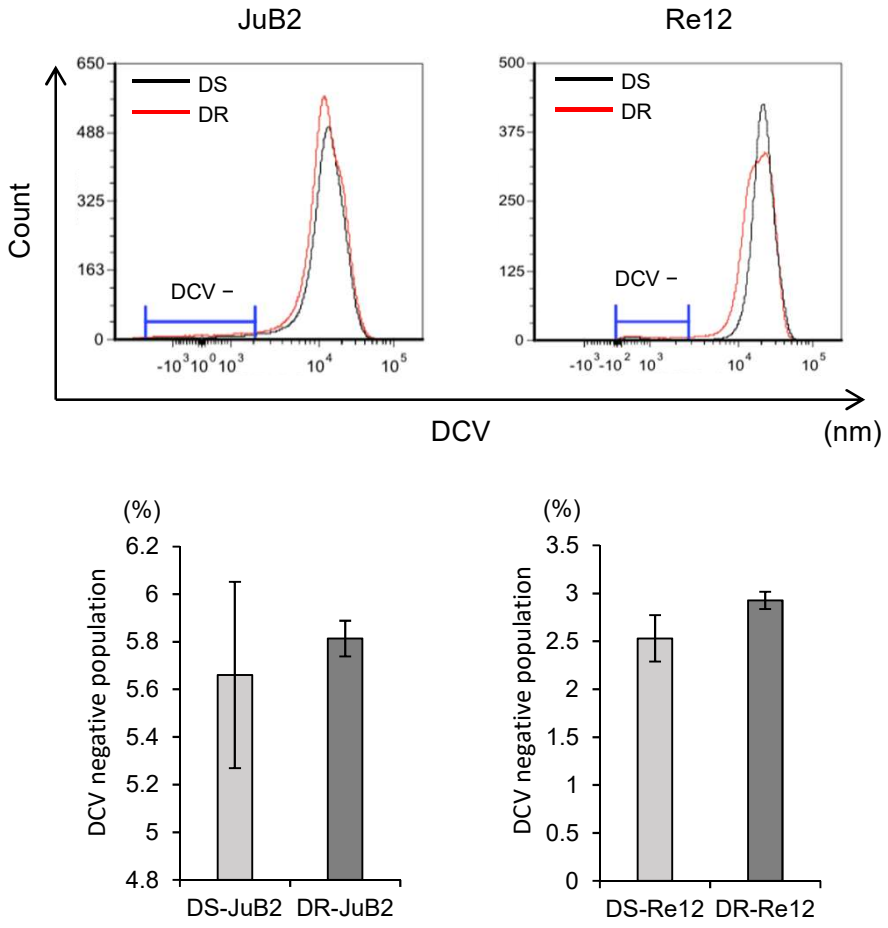

Fig. S1 Morita *et al.*

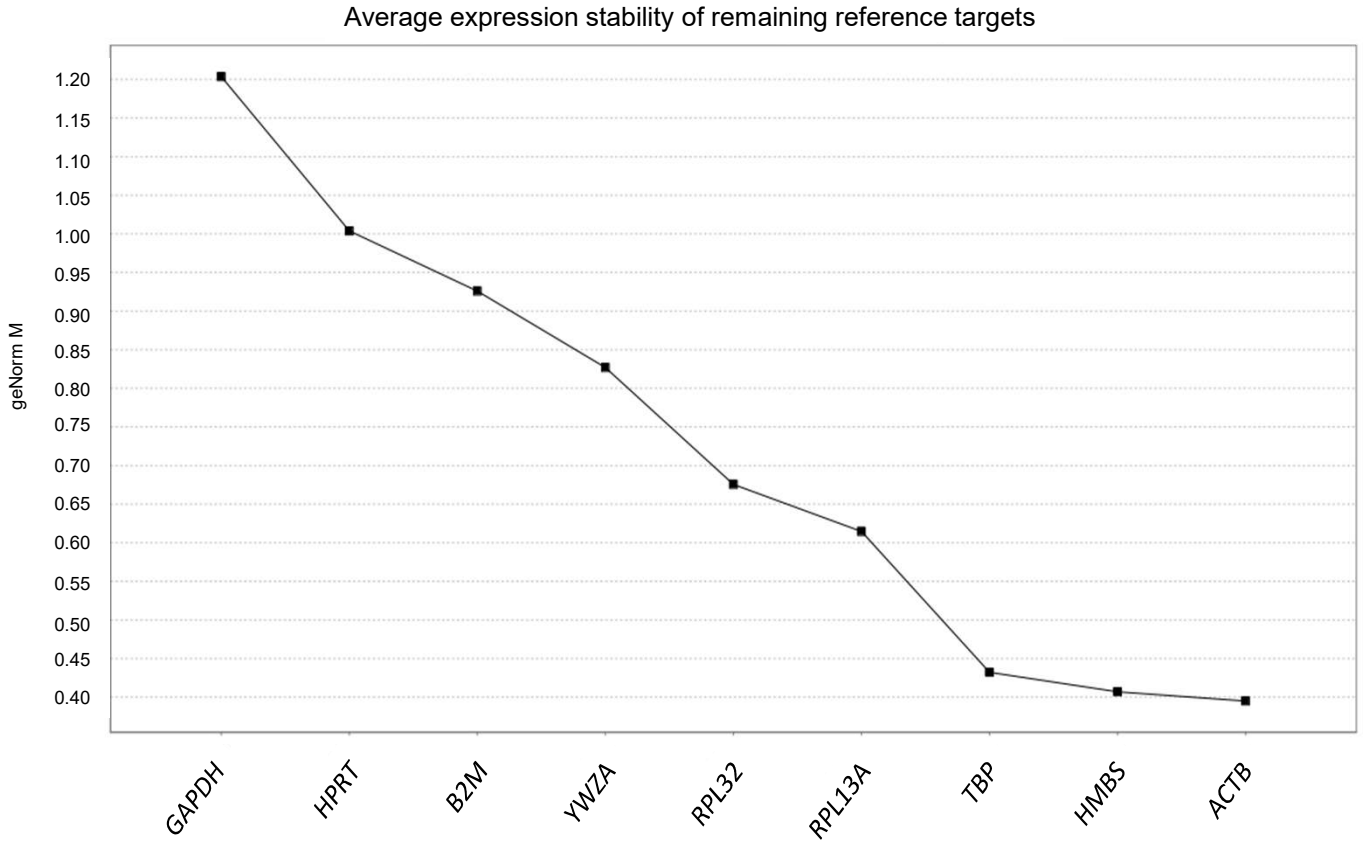

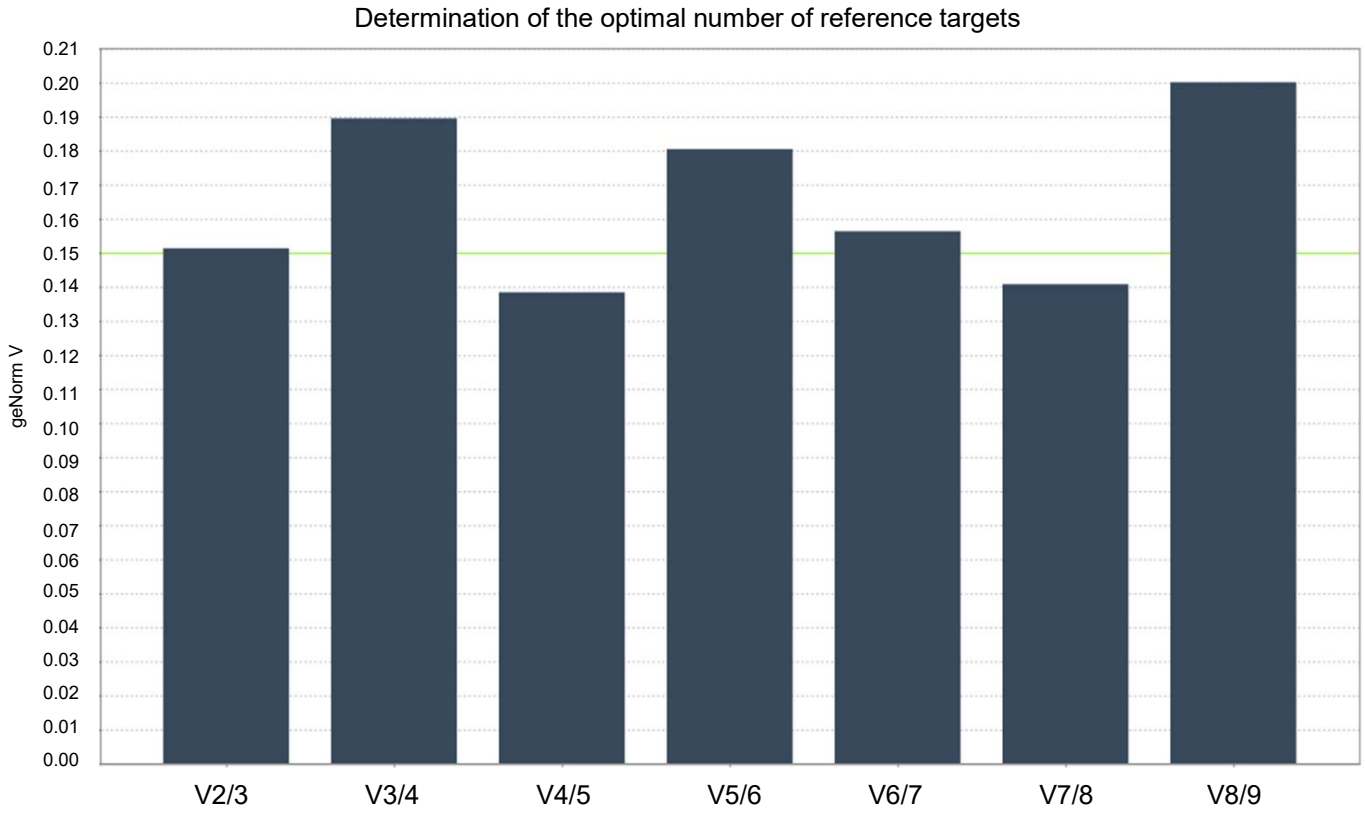

Fig. S2 Morita *et al.*

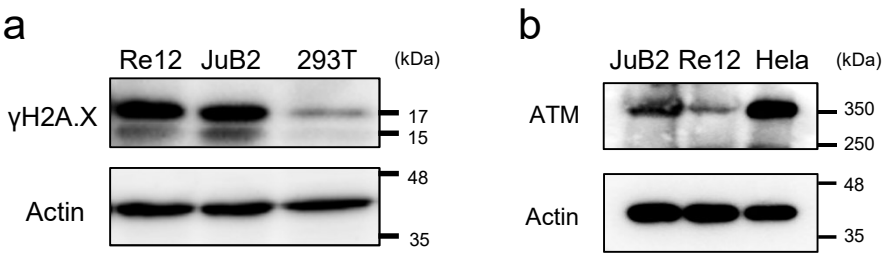

Fig. S3 Morita *et al.*